Encapsulation of folic acid in different silica porous supports: a comparative study

Édgar Pérez-Esteve,[a*] María Ruiz-Rico,[a] Cristina de la Torre,[b,c] Luis A. Villaescusa,[b] Felix Sancenón,[b,c] María D. Marcos,[b,c] Pedro Amorós,[d] Ramón Martínez-Máñez,[b,c] José Manuel Barat[a]

[a] Grupo de Investigación e Innovación Alimentaria, Universitat Politècnica de València. Camino de Vera s/n, 46022, Valencia, Spain

[b] Centro de Reconocimiento Molecular y Desarrollo Tecnológico (IDM), Unidad Mixta Universitat Politècnica de València – Universidad de Valencia. Departamento de Química Universitat Politècnica de València, Camino de Vera s/n, 46022, Valencia, Spain

[c] CIBER de Bioingeniería, Biomateriales y Nanomedicina (CIBER-BBN)

[d] Institut de Ciència dels Materials (ICMUV), Universitat de València, P.O. Box 2085, 46071, Valencia, Spain

* Corresponding author. Tel.: +34 963877365. E-mail address: edpees@upv.es (E. Pérez-Esteve)

ABSTRACT

Although folic acid is essential to numerous bodily functions, recent research indicates that a massive exposition to the vitamin could be a double-edged sword. In this study, the capacity of different caped mesoporous silica particles (i.e. Hollow Silica Shells, MCM-41, SBA-15 and UVM-7)

to dose FA during its passage through the gastrointestinal tract has been evaluated. Results confirmed that the four capped materials were capable to hinder the delivery of FA at low pH (i.e. stomach) as well as able to deliver great amounts of the vitamin at neutral pH (i.e. intestine). Nevertheless, the encapsulation efficiency and the deliver kinetics differed among supports. While supports with large pore entrance exhibited an initial fast release, MCM-41, showed a sustained release along the time. This correlation between textural properties and release kinetics for each of the supports reveals the importance of a proper support selection as a strategy to control the delivery of active molecules.

Keywords: Folic acid; porous silica supports; smart delivery; nutrition; optimization

1. Introduction

Folates have been, and remain, a subject of ongoing research due to their numerous bodily functions, including DNA synthesis and repair, cell division and cell growth. Folates exist in a large variety of foods including green leafy vegetables, fruits, meat products, beans, fermented dairy products, and cereals. However, folates are sensitive to physical factors such as temperature, pressure, and exposure to light and can be affected during food processing or digestion (Nasr Hage, Jalloul, Sabbah & Adib, 2012) so that folate deficiencies occur worldwide. Folate deficiency is of such importance to humans that it can cause neural tube defects in developing embryos, elevated plasma homocysteine, different types of cancer, Alzheimer, etc. (Nguyen & Hendrickx, 2003; Kotsopoulos, Kim & Narod, 2012; Hinterberger & Fischer, 2013; Lubecka-Pietruszewska, Kaufman-Szymczyk, Stefanska & Fabianowska-Majewska, 2013). To maintain an adequate folate status a diet supplementation with FA from fortified foods or nutritional supplements is generally recommended in many countries, especially during pregnancy.

Although there are irrefutable evidences about the benefits of FA supplementation, recent studies suggest that a massive exposition to high bioavailable FA leads to the direct appearance of untransformed FA in the systemic circulation. The presence of unmetabolized FA in blood has been lately related to certain cancer development, cardiovascular disease, anaemias… (Kotsopoulos et al., 2012). In this context, encapsulation methods to prevent environmental degradation of folates as well as to control the release along the digestive tract (i.e. no delivery in the stomach –pH 2-, and a sustained release in the intestine –pH 7.5) seems to be a convenient strategy to solve problems related to FA deficiency, while avoiding problems related with massive exposition to the vitamin.

From another point of view, the development of nanotechnology is opening new areas for exploration in the design of smart delivery systems. In particular several nanodevices have been suggested to provide a benefit to the drug delivery scene. Among potential drug-delivery

supports, mesoporous silica particles (MSPs) have been widely proposed as delivery systems in various life science fields such as medicine, nutrition, and food technology in recent years (Wang, Wu, Chen & Lin, 2009; Mondragón et al., 2014).

Periodically ordered mesoporous silicas, created by combining surfactant micellar aggregates with reactive silica precursors, were discovered about 20 years ago by researchers at Mobil (Beck *et al.*, 1992). This first class of periodic mesoporous silicas were known as M41S phases. Since these seminal studies, fine tuning of the reaction parameters such as concentrations, pH value, chemical nature of the surfactants, temperature, and time has allowed a precise adjustment of size, morphology, and pore structure and the development of different MSPs such as MCM-41, SBA-15, UVM-7, etc (Argyo, Weiss, Bräuchle & Bein, 2013; Pérez-Esteve *et al.*, 2014). MSPs are characterized by a high homogeneous porosity defined from tunable pores with size between 2 to 10 nm, that make these scaffolds ideal for hosting functional guest molecules. Moreover it has been reported that the surface of ordered silicas can be functionalised with molecular/supramolecular ensembles to develop gated-MSPs, which show “zero delivery” yet can release their cargo on-command in response to specially designed external stimuli (Aznar, Martínez-Máñez, Sancenón, 2009). This opens the possibility to design stimuli-responsive mechanisms with spatiotemporal control of cargo release (Argyo *et al*., 2013). In particular, polyamines are well-known pH-responsive molecules able to adopt different conformations as a consequence of changes in the pH, and this characteristic has been applied to the design of pH-responsive gated materials (Bernardos et al., 2008).

In this work, encapsulation of large amounts of FA in the final delivery systems is very important to minimize the quantity of material needed to provide the Recommended Dietary Intake or a percentage of the same. Moreover, to control the FA release rate is very important to avoid absorption peaks. In this manner, the most suitable delivery system to modulate FA bioaccessiblity along the gastrointestinal tract should be able to hinder FA release in the stomach,

and achieve a sustained release before arriving to the jejunum where FA is absorbed (i.e. first 2h of the intestinal phase of the digestion) (Baker, Thomson, Feingold & Frank, 1969). It is well known that in mesoporous materials both, loading efficiency as well as release rate, depend on properties of the support such as surface area, pore size, pore geometry, total pore volume, surface chemistry as well as on the loading procedure.

Based in these concepts, the aim of this work was the evaluation of different silica supports (MCM-41, SBA-15, UVM-7 and hollow silica microspheres) caped with pH-responsive molecular gates to encapsulate sufficient amount of FA and to achieve a controlled and sustained release of the vitamin under digestive conditions. To reach this goal studies on loading optimization, encapsulation capacity, release kinetics and biocompatibility of the delivery systems with different cell lines have been performed.

2. Materials and methods

2.1 Chemicals

Tetraethylorthosilicate (TEOS), *N*-cetyltrimethylammonium bromide (CTABr), pluronic P123 (P123), triethanolamine ($TEAH_3$), sodium hydroxide (NaOH), hydrochloric acid (HCl), acetic acid and *N*-(3-trimethoxysilylpropyl)diethylenetriamine (N3), sodium phosphate monobasic (NaH_2PO_4), sodium phosphate dibasic (Na_2HPO_4), tetrabutylammonium hydrogen sulfate (TBAHS), deuterium oxide (D_2O), sodium deuteroxide(NaOD) and all chemicals for the digestive fluids were provided by Sigma (Sigma-Aldrich Química S.L., Madrid, Spain). Folic acid was purchased from Schircks Laboratories (Jona, Switzerland). Acetonitrile HPLC grade was provided by Scharlau (Barcelona, Spain). Hollow Silica Shells were provided by Exilica Limited (Coventry, UK). Tetraethyl ammonium bromide (>99%) was provided by Merck (Darmstadt, Germany).

For cell culture experiments, trypan blue solution (0.4%) cell culture grade and DMSO, PBS and Dulbecco's Modified Eagle's medium (DMEM) with glucose, L-glutamine and pyruvate for cell culture were provided by Sigma-Aldrich. Mc Coy's 5a Medium and Keratinocyte Serum Free Medium, Fetal Bovine Serum (FBS) and trypsin were purchased from Gibco (Life Technologies, Madrid, Spain). Cell proliferation reagent WST-1 was purchased from Roche Applied Science (Barcelona, Spain).

2.2 Mesoporous silica particles synthesis

Microparticulated MCM-41 particles (**M**) were synthesized following the so-called "atrane route", according to the method described by Bernardos *et al.* (2008). CTABr was used as the structure-directing agent. The molar ratio of the reagents was fixed to 7 $TEAH_3$: 2 TEOS: 0.52 CTABr: 0.5 NaOH: 180 H_2O. CTABr was added to a solution of $TEAH_3$ containing NaOH and TEOS at 118 °C. After dissolving CTABr in the solution, water was slowly added with vigorous stirring at 70 °C.

After a few minutes, a white suspension was formed. This mixture was aged in an autoclave at 100 °C for 24h.

SBA-15 microparticles (**S**) were synthesized following the method reported by Zhao, Huo, Feng, Chmelka & Stucky (1988). P123 was used as the structure-directing agent. The molar ratio of the reagents was fixed to: 0.017 P123: 1.0 TEOS: 6 HCl: 196 H_2O. The preparation was performed by mixing an aqueous solution of P123 with HCl solution, and stirring for 2 h, after which the silica source, TEOS, was added. This final mixture was stirred for a further 24 h. The mixture was aged in an autoclave at 100 °C for 24h.

UVM-7 particles (**U**) were synthesised following the method presented by Comes *et al.* (2009), based also on the "atrane route". The molar ratio of the reagents was fixed at 7 $TEAH_3$: 2 TEOS: 0.52 CTABr: 180 H_2O. The TEOS/$TEAH_3$ mixture was heated to 120 °C in a Dean-Stark until no elimination of ethanol was observed. The mixture was cooled to 90 °C and CTABr was added gradually in small portions, followed by dilution with water. The mixture was aged for 24 h.

For all samples, the resulting powder was recovered by centrifugation, washed with deionised water, and air-dried at room temperature. To prepare the final mesoporous materials, the as-synthesized solids were calcined at 550 °C using an oxidant atmosphere for 5 h in order to remove the template phase.

2.3 Folic acid loading and amine functionalization

10 different FA loaded and functionalised solids were prepared for each support. In a typical synthesis, 0.5 mL of an aqueous solution of FA in phosphate buffer (PBS) (10 mg/mL) was dropped to 100 mg of the corresponding support (i.e. MCM-41, SBA-15, UVM-7 and Hollow Silica Shells) and mixed. After the impregnation, solids were dried at 30 °C to eliminate water content. The procedure was repeated as many times as needed to obtain solids with a sequential number of impregnation cycles from 1 to 10.

To obtain the final loaded and functionalised solids, 100 mg of each of the FA-loaded supports were suspended in 10 mL of an aqueous solution of acetic acid (5%) and an excess of N3 (0.43 mL, 0.015 mmol) was added. The final mixtures were stirred for 5.5 h at room temperature. The forty loaded and functionalized solids (H1-10, M1-10, S1-10 and U1-10) were isolated by vacuum filtration, washed with 300 mL of water adjusted to pH 2, and dried at room temperature for 24 h. To evaluate the efficiency of the different impregnation cycles, the "relative loading efficiency" was calculated (see section 2.5).

2.4 Characterization

X-ray diffraction (XRD), transmission electron microscopy (TEM), field emission scanning electron microscopy (FESEM), N_2 adsorption-desorption, thermogravimetric analysis (TGA), ^{1}H NMR, laser diffraction and Z-potential measurements were employed to characterize the synthesized supports.

XRD were performed on a Bruker D8 Advance diffractometer (Bruker, Coventry, UK) using CuKα radiation. TEM images were obtained with a JEOL JEM-1010 (JEOL Europe SAS, Croissy-sur-Seine, France). FESEM images were acquired with a Zeiss Ultra 55 (Carl Zeiss NTS GmbH, Oberkochen, Germany) and observed in the secondary electron mode.

N_2 adsorption-desorption isotherms were recorded with a Micromeritics ASAP 2010 automated sorption analyser (Micromeritics Instrument Corporation, Norcross, USA). The samples were degassed at 120 °C in vacuum overnight. The specific surface areas were calculated from the adsorption data in the low pressure range using the BET model. Pore size was determined following the BJH method. From the XRD and porosimetry studies, the a_0 cell parameter and wall thickness of the different supports were calculated.

The theoretical maximum loading capacity in the different supports was calculated by dividing the value of pore volume of each of the supports by the value of FA molecule volume (1.16 nm^3) and assuming that in a highly efficient packaging FA could lead to a maximum occupancy of ca. 75% of the supports total pore volume (Pérez-Esteve *et al.*, 2015).

The composition of loaded and functionalised supports was determined by TGA and ^{1}H NMR. Thermogravimetric analyses were carried out on a TGA/SDTA 851e Mettler Toledo balance (Mettler Toledo Inc., Schwarzenbach, Switzerland), using an oxidant atmosphere (air, 80 mL/min) with a heating program consisting of a heating ramp of 10 °C per minute from 393 to 1273 K and an isothermal heating step at this temperature for 30 min. ^{1}H NMR spectra were recorded at RT using a Bruker AV400 spectrometer (Bruker Daltonik GmbH, Bremen, Germany) after dissolving the corresponding sample in NaOD/D_2O in the presence of tetraethyl ammonium bromide as internal standard.

The particle size distribution of the different bare and functionalised MSPs was determined using a Malvern Mastersizer 2000 (Malvern Instruments, Malvern, UK). For the measurements, samples were dispersed in distilled water. Data analysis was based on the Mie theory using refractive indices of 1.33 and 1.45 for the dispersant and MSPs, respectively. An adsorption value of 0.001 was used for all samples. Variation of this adsorption value did not significantly alter the obtained distributions. Measurements were performed in triplicate.

To determine the zeta potential (ζ) of the bare and functionalised MSPs, a Zetasizer Nano ZS equipment (Malvern Instruments, Malvern, UK) was used. Samples were dispersed in distilled water at a concentration of 1 mg/mL. Before each measurement, samples were sonicated for 2 minutes to preclude aggregation. The zeta potential was calculated from the particle mobility values by applying the Smoluchowski model. The average of five recordings was reported as zeta potential. The measurements were performed at 25 °C. Measurements were performed in triplicate.

2.5 FA release kinetics and loading efficiency evaluation

To obtain the FA release kinetics for each of the 40 solids at different pHs, 10 mg of the corresponding solids were placed in 25 mL of water at pH 2 (simulating condition at the stomach) and pH 7.5 (simulating condition at the intestine). At a certain times aliquots were separated, the suspension filtered and the solution analysed by HPLC.

The "relative loading efficiency" for each solid was calculated according to the following equation:

$$\text{Relative loading efficiency (\%)} = FA_D/FA_L \times 100$$

where FA_D are the mg of FA delivered per 1mg of loaded solid at pH 7.5 after 4 h and FA_L are the mg of folic acid employed for the loading of 1 mg of the corresponding solid.

The FA release kinetics from pore voids of the porous silica supports were calculated using the Higuchi model where the amount of guest release, Q_t, per unit of exposed area at time *t* can then be described by the following equation

$$Q_t = k_H \sqrt{t}$$

where k_H is the release rate constant for the Higuchi model.

2.6 Folic acid quantification

FA was quantified by reversed-phase gradient HPLC method according to the method described by Pérez-Esteve *et al.* (2015). The HPLC instrument consisted of a Hitachi LaChrom Elite liquid chromatograph (Hitachi Ltd., Tokyo, Japan) equipped with an auto-sampler and UV detector (model L-2400). A Kromaphase 100 C18 (250 mm x 4.6 mm i.d., 5 μm particle size analytical column) (Scharlau, Barcelona, Spain) was used for the separations. The mobile phase consisted of (A) 0.125 mM of NaH_2PO_4, 0.875 mM of Na_2HPO_4 and 0.4mM of TBAHS in water and (B) acetonitrile-phase A 65:35 (v/v). The gradient program was as follows: 0 to 5 min, 90% A and 10%

B; thereafter, the proportion of B was increased linearly to reach 36% at 15 min and 60% at 30 min. After that, decreased linearly to reach 10% at 35 min and remained in the initial conditions for 5 min.

2.7 Cell culture Conditions

HeLa human cervix adenocarcinoma and HEPG2 human liver carcinoma were grown in DMEM supplemented with 10% FBS. HCT116 human colon carcinoma cells were grown in McCoy's 5a Medium Modified supplemented with 10% FBS and HK2 homo sapiens kidney papilloma cells were grown in Keratinocyte Serum Free Medium supplemented with bovine pituitary extract (BPE) and human recombinant epidermal growth factor (EGF). All of these cells were purchased from the German Resource Centre for Biological Materials (DSMZ). Cells were maintained at 37 °C in an atmosphere of 5% carbon dioxide and 95% air and underwent passage twice a week.

2.8 WST-1 Cell viability Assay

HeLa, HCT116, HEPG2 and HK2 cells were cultured in sterile 24-well plates at a density of $2 \cdot 10^4$ cells/well for HeLa and HK2 and $2 \cdot 10^5$ for HCT116 and HEPG2 in a 1000 μL of respectively grown medium and were incubated 24 h in a CO_2 incubator at 37 °C. Then, solids in DMSO were added to cells in quadruplicate at final concentrations of 50, 100, 150 and 200 μg/mL. Control wells did not contain any solid. After 23 h, cells were washed with PBS and then 30 μL of WST-1 reagent were added to each well and were incubated during 1 h, a total of 24 h of incubation was therefore studied. Before reading the plate, cells shacked for 1 min to ensure homogeneous distribution of colour. Then the absorbance was measured at a wavelength of 450 nm and 690 nm in VICTOR X5 PerkinElmer. Results are expressed as an average of the results of three independent experiments.

2.9 Data analysis

The results of the FA delivery from the different solids prepared were statistically processed using Statgraphics Centuriun XV (Manugistics Inc., Rockville, MD, USA). Statistical analysis on FA concentrations was made using an analysis of variance (One-Way ANOVA). The LSD (least significant difference) procedure was utilised to test for differences between averages at the 5% significance level.

3. Results and discussion

3.1 Design, synthesis and characterization of the gated supports

Incorporation of gate-like ensembles into porous silica particles is a suitable approach to design devices for controlled delivery applications. The development of responsive gated materials requires selecting two components: (i) a suitable gate-like ensemble that changes one or several properties (size, shape, bulkiness, charge, etc.) upon external stimuli and (ii) the selection of the nano-structured matrix in which the gate-like scaffold is grafted. In this wok we have selected a diethylenetriamine moiety as capping ensemble due to its proved properties to control the delivery of cargo molecules from the void of mesoporous silica particles as a response of pH changes (Bernardos *et al.*, 2008; Casasús *et al*., 2008; Pérez-Esteve *et al.*, 2015). Moreover as inorganic support, we have selected four different porous silica supports (MCM-41, UVM-7, SBA-15 and Hollow Silica) having different size, shape and pore system. In all cases, the particle size was in the microscale. The MCM-41 support (M), the most popular member of the M41S family, is characterized by a regular pore system which consists of a hexagonal array of unidimensional, hexagonally shaped pores (Grün, Unger, Matsumoto & Tsutsumi, 1999). The UVM-7 support (U) can be described as bimodal porous silica constructed by the aggregation of pseudo-spherical mesoporous primary nanoparticles. The intra-nanoparticle pore system consists of regular-sized

mesopores disposed in a pseudo-hexagonal disordered array, while the arrangement of the inter-particle meso/macropores exhibits xerogel-like characteristics (Pérez-Cabrero *et al.*, 2012). Microparticulated SBA-15 (S) presents uniform hexagonal pores with a narrow pore size distribution and a tunable pore diameter between 5 and 15 nm. The thickness of the framework walls is about 3.1 to 6.4 nm, which gives the material a higher hydrothermal and mechanical stability (Thielemann, Girgsdies, Schlögl & Hesscorresponding, 2011). Finally, Hollow Silica Shells were employed due to their reported high storage capacity of its hollow core structure (Zhu, Shi, Shen, Chen, Dong & Ruan, 2005). According to these reported textural features, FA (which measures 1 x 1.45 nm) might be easily encapsulated in the four selected supports (Pérez-Esteve *et al.*, 2015).

Once synthesized (M, S, U) or acquired from the supplier (H), solids were characterized by using standard procedures. XRD patterns of each of the supports can be found in Supplementary Figure 1. Figure S1H shows the diffractogram of the commercially available Hollow Silica Shells. As observed, at low angles there were no reflections suggesting the absence of any order in the pore structure. XRD at high angles revealed a broad peak around 22 (2θ) (data not shown), indicating that employed H support presents an amorphous structure. X-ray patterns of the MCM-41, SBA-15 and UVM-7 as synthesized, calcined and loaded with FA and functionalized with amines are shown in Figures S1M, S1S and S1U respectively. Figure S1M shows the four typical peaks of a hexagonal ordered array, indexed as (100), (110), (200) and (210) Bragg reflections, of the as-synthesised MCM-41 material. An a_0 cell parameter of 41.7 Å (d_{100} spacing = 36.1 Å) was calculated. A significant shift of the (100) reflection in the XRD powder of the MCM-41 calcined sample was clearly appreciated, corresponding to a cell contraction (5.6 Å) related to condensation of silanols during the calcination step. The loaded and capped final material showed that reflections (110), (200) and (210) were lost, most likely due to a reduced contrast that can be attributed to the presence of FA in the pore voids and the anchored polyamine molecule.

298 Nevertheless, the existence in all cases of the (100) peak in the XRD patterns indicated that the
299 process of pore loading with FA, and the additional functionalization with the polyamine, did not
300 modify the typical porosity of the mesoporous MCM-41 scaffold. Figure S1S shows a sharp peak at
301 ca. 0.9, indexed as the (100) reflection, and two minor reflections in the 1.0–2.0 interval, indexed
302 as (110) and (200) Bragg reflections, respectively. These peaks were indexed according to two-
303 dimensional hexagonal *p6mm* symmetry, of a well-defined SBA-15 mesostructure. Hence, the
304 obtained a_0 cell parameter was 113.47 Å (d_{100} spacing =98.27 Å). The calcination process displaced
305 the (100) reflection due to condensation of silanol groups, resulting a cell contraction of 10.5 Å.
306 The preservation of (100) in the final solid indicated that the long-range hexagonal symmetry of
307 SBA-15 was maintained after FA loading and amine functionalization. Finally, figure S1U shows
308 two broad low-angle reflections that could be related with a disordered hexagonal array of the
309 mesopores in this UVM-7 support. Assuming the first peak could be indexed as the (100)
310 reflexion, an a_0 cell parameter of 47.54 Å (d_{100} spacing =41.18 Å) was obtained. The XRD pattern of
311 the calcined UVM-7 solid showed a displacement of the (100) peak. It indicated a cell contraction
312 of approximately 3.1 Å. The X-ray diffraction patterns of the FA loaded and polyamine-
313 functionalised solid was characterized by the presence of an intense peak at ca. 2 (100 reflection)
314 typical of a surfactant-assisted mesoporous material, indicating that neither the loading nor the
315 functionalization induced any significant effect on the mesoporous structure of the silica matrix.
316 As a complement to XRD patterns to elucidate porous structure of different supports, Figure 1
317 shows FESEM and TEM images of the different silica support used in this study. By means of
318 FESEM observation, a characterization of the shape of the particles was performed. All different
319 supports showed sizes in the micro-scale. These pictures also confirmed that different particles
320 exhibited diverse morphology, from completely spherical particles (H), to irregular shaped
321 particles (M), elongated particles (S) or agglomeration of nanoparticles (U). The comparison of the
322 pictures before and after loading with FA and functionalization with N3 for the same support

allowed concluding that neither loading nor functionalization significantly modified the appearance of the external surface suggesting none deposition of FA on the surface, and thus a complete encapsulation of FA in the support.

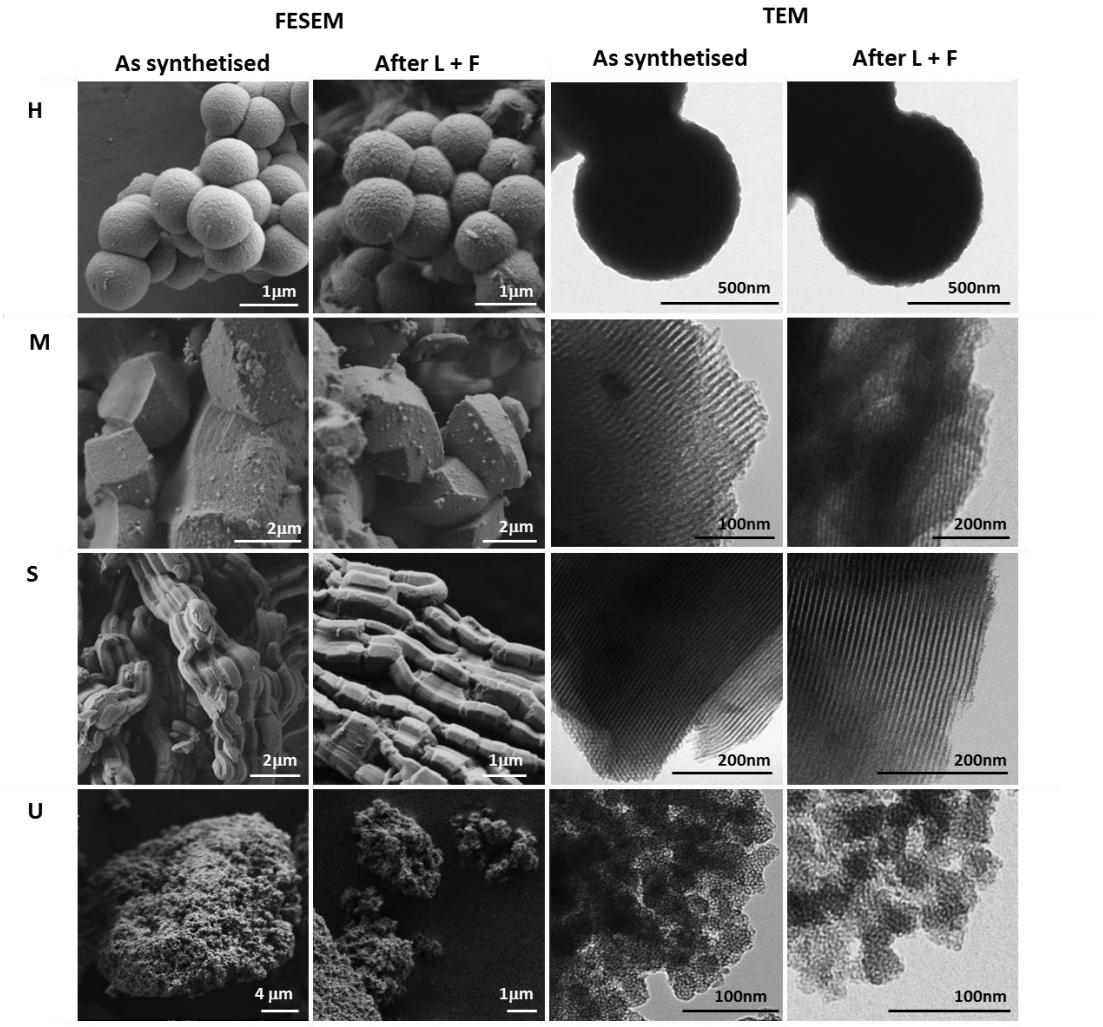

Figure 1. Characterization of particle size, particle shape and pore system by means of FESEM and TEM. Hollow Silica Shells (H), MCM-41 (M), SBA-15 (S) and UVM-7 (U).

The presence of mesostructures on MCM-41 (M), SBA-15 (S) and UVM-7 (U) after loading with FA and functionalization with polyamines was confirmed by TEM images. Figure 1 shows the typical channels of the mesoporous matrixes either as alternate black and white stripes or as pseudo hexagonal arrays of pore voids. These channels were visualised not only in the starting calcined materials but also in final FA-loaded and N3-functionalised supports, confirming the preservation of the mesopores during the preparation process. Moreover, TEM observations revealed the absence of any clear mesostructure in Hollow Silica Shells (H) particles.

N_2 adsorption-desorption isotherms of the starting and final silica supports are shown in Supplementary Figure 2. Figure S2H shows the N_2 adsorption–desorption isotherms of Hollow Silica Shells. No capillary condensation was detected in the isotherms, confirming the absence of mesopores suggested by XRD and microscopy observations. Nevertheless, the high loading capacity exhibited by this material (see section 3.2) made us think that the sample might have accessible microcavities where FA can be clearly entrapped.

Figures S2M and S2U show the isotherms of the MCM-41 and UVM-7 systems, respectively. In both cases the starting materials exhibited a sharp and well defined adsorption step at relative pressure values between 0.2 and 0.6, attributed to nitrogen condensation in the mesopore inlets. The absence of a hysteresis loop in this interval and the narrow BJH pore distribution suggested the existence of uniform cylindrical mesopores. The difference between MCM-41 and UVM-7 was that the curve of UVM-7 showed two steps. The first, as commented, was originated from the capillarity condensation of N_2 into the mesopores, whereas the second, at higher relative pressures, was related to the filling of textural interparticle pores typical of the UVM-7 scaffolding. According to IUPAC definition, both isotherms are type IV, characteristic of mesoporous materials with narrow pore size distributions. Finally, Figure S2S shows a type IV isotherm with adsorption step at relative pressure around 0.6, typical of SBA-15 particles with well-defined channel-like mesopores. Moreover, we have applied the Barrett-Joyner-Halenda

(BJH) model on the adsorption curves of the isotherms to calculate pore diameter and pore volume of all solids. In addition, the application of the Brunauer, Emmett and Teller (BET) model allowed the calculation of total specific surface. Calculated values for different supports are shown in Table 1. MCM-41 and UVM-7 have a similar surface area of ca. 1000 $m^2 \cdot g^{-1}$ and a mesoporous size of ca. 2.6 nm. In contrast, SBA-15 has lower surface area but a larger pore size of ca. 8 nm. Surface of Hollow Silica Shells was very low compared with the other supports due to the confirmed absence of mesoporosity.

For all supports, a change on the N_2 adsorption-desorption isotherms for the corresponding FA-loaded and N3-functionalized supports was observed. In particular, isotherms showed no remarkable steps at low-intermediate relative pressure indicating a decrease of surface area and volume after FA loading and amine functionalization (Supplementary Figure 2).

Textural properties of different supports calculated from nitrogen adsorption-desorption isotherms and XRD are summarized in Table 1. Table 1 also shows the calculated theoretical maximum loading capacity for M, S and U.

Table 1. Textural properties of calcined silica matrixes: Hollow Silica Shells (H), MCM-41 (M), SBA-15 (S) and UVM-7 (U).

Silica Support	Area[a] ($m^2 \cdot g^{-1}$)	Mesopore (P/P0<0,6)		Textural pore (P/P0>0,6)		a_0[c] (nm)	dw[d] (nm)	TMLC[e] (μg/mg)	
		Pore volume[b] ($c^3 \cdot g^{-1}$)	Pore size[b] (nm)	Pore volume[b] ($c^3 \cdot g^{-1}$)	Pore size[b] (nm)				
H	258	-	-	-	-	[f]	[f]	-	
M	1074	0.91	2.61	-	-	4.54	1.93	431	
S	649	0.92	7.89	-	-	10.54	2.64	436	
U	919	0.75	2.65	1.10	54.80	4.75	2.10	355	(876)[g]

a. BET specific surface values calculated from the N_2 adsorption branch of the isotherms.
b. Pore volumes and pore sizes (diameter) calculated from the N_2 adsorption-desorption isotherms for selected materials.
c. Cell parameter. $a_{0=}2d_{100} \cdot (\sqrt{3})^{-1}$
d. Wall thickness. $dw = a_0 - d_p$, where d_p is the mesopore pore diameter
e. Theoretical maximum loading capacity
f. Without available data from XRD.
g. TMLC calculated from textural pore

Particle size is important when designing devices for oral control release. It is well known that nanoparticles' cellular uptake is size-dependant. In particular it has been reported that nanoparticles larger than 600-1000 nm exhibit a notable lower transport across the follicle-associated epithelium when compared with smaller particles (He, Yin, Tang & Yin, 2012). According to these data, all the final supports are suitable for oral delivery purposes and are not expected to be absorbed in the digestive tract. Size distribution of the four supports in all the stages of their preparation, from the bare particles to the particles loaded with FA and functionalised with the N3 polyamine is shown is Supplementary Figure 3. Three of the supports (H, M and S) did not change significantly their grain size as a function of the loading and functionalization. However, U grains which are composed of an agglomeration of porous nanoparticles changed dramatically its size after the functionalization with the polyamine. This change was attributed to the deflocculant effect of the functionalization process. During functionalization process the vigorous stirring provoked grain desegregation. The subsequent functionalization with amines increases the stability of desegregated grains by adding positive charges to the surface (Pérez-Esteve et *al*., 2014). This cooperative effect results in the reduction of U grain size, also detected in FESEM observations (Figure 1U). In this manner, after the loading and functionalization process, all the solids exhibited a particle size of ca. 0.6-1 micron.

Finally, the efficiency of functionalization was tested by zeta potential determinations. It is generally accepted that mesoporous silica is negatively charged above the isoelectric point (pH 2-3). These values agree with those measured for all the four starting particles. As it can be seen in Supplementary Figure 4, unloaded H, M, S, U exhibited negative zeta potential values in the -50 mV to -30 mV range. The loading of the supports with FA did not modify significantly zeta potential values. However, the functionalization of the loaded supports with the polyamine N3 transformed the zeta potential from negative to positive (ca. +30 mV), confirming that the functionalization successfully occurred in all cases. Moreover we also found that the number of

413 loading cycles (vide infra) did not cause remarkable changes on final zeta potential values for the
414 different particles.
415
416 ***3.2 Loading efficiency evaluation***
417 With the objective of evaluating the loading capacity of the silica supports with FA, different
418 experiments were carried out. For each of the supports, 10 solids impregnated from 1 to 10 times
419 with 0.5 mL of an aqueous solution of FA in PBS (10 mg/mL) were prepared.
420 FA content in prepared solids was determined by TGA and ^{1}HNMR. Supplementary Table 1 shows
421 content of organic matter (α) in solids impregnated 10 times as well as in those with the highest
422 (FA released):(FA employed in the loading of the support) ratio, called optimized solids (vide
423 infra). For all the supports, the higher the impregnation cycles, the higher the content in FA. N3
424 content was larger for solids S and U, than for H and M. For the same support, content of N3
425 (expressed in mg N3/mg SiO_2) did not change as a function of the number of loading cycles.
426 Comparing the calculated theoretical maximum loading capacity (see Table 1) with real FA
427 content it was shown that M and S were able to reach after 10 impregnation cycles ca. 60% of the
428 maximum content, while U incorporated ca. 70%. These results point that the loading procedure
429 employed for FA loading (i.e. impregnation) is very efficient.
430 Release effectiveness of each solid was also evaluated by determining the maximum amount of
431 FA delivered at pH 7.5. Figure 2 shows FA delivered (μg FA/mg solid) from each of the 40 solids
432 prepared after reaching the equilibrium (2h). As it can be seen, for each of the different supports,
433 the more impregnation cycles employed, the more FA delivery was achieved. In no case a
434 saturation of the loading capacity seems to be achieved, since the slope described by the bars for
435 each of the impregnation cycles does not reach the horizon. These data confirm that the
436 theoretical maximum loading capacity was not achieved in any of the supports.

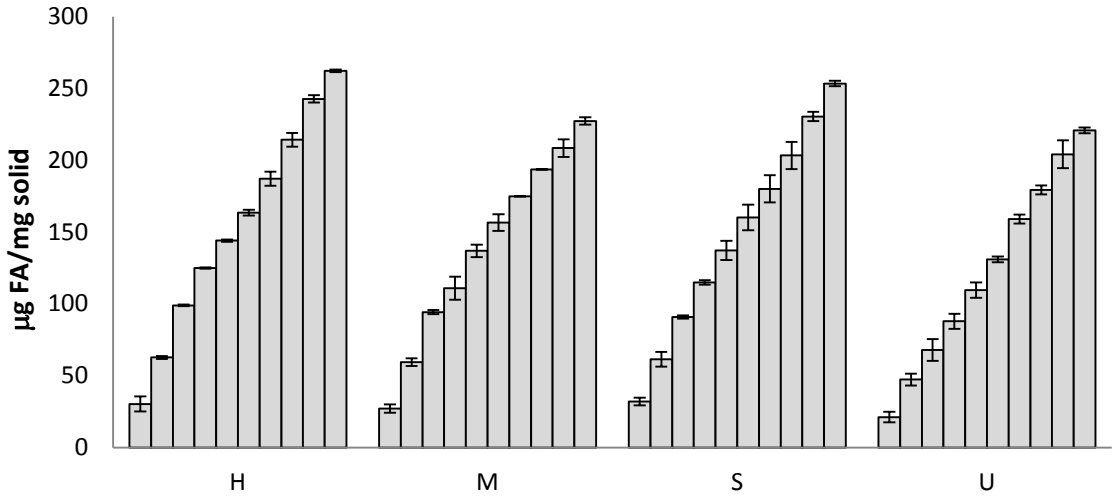

Figure 2. Maximum FA delivery (µg FA/mg solid) for different solids impregnated from 1 to 10 times (ordered sequentially) and functionalized with N3. Hollow Silica Shells (H), MCM-41 (M), SBA-15 (S) and UVM-7 (U). Values are Means±SD, n=3.

Comparing the maximum amount of FA delivered for the different supports after 10 loadings, it can be seen how Hollow Silica Shells (H) was the support that exhibited the maximum FA delivery (262 µg FA/mg solid) followed by SBA-15 (ca. 252 µg FA/mg solid), MCM-41 (227 µg FA/mg solid) and UVM-7 (220 µg FA/mg solid). These values represent a percentage of release of 96, 91, 95 and 85% of the loaded FA for H, M, S and U supports, respectively. These high values indicate that the release of FA from the voids of the studied supports is very efficient, probably due to a very low interaction among FA (charged negatively at pH 7.5) and the inner surface of the supports (also charged negatively at pH 7.5).

Finally and with the objective of determine the relative loading/delivery performance of the solids from a technological efficiency point of view the “relative loading efficiency” (RLE) was calculated. This parameter was calculated by determining the ratio between the amount of FA delivered (after 4h at pH 7.5) per mg of loaded solid and the mg of FA used for loading 1 mg of the support (see Experimental Section for details).

Figure 3 shows RLE values for different solids impregnated from 1 to 10 times with FA and functionalized with N3. As observed, each support exhibited a different behaviour according to the relative loading efficiency. S was the support with larger RLE, probably due to its higher pore size and pore volume. H also exhibited a high RLE, similar to M in the first impregnation cycles. Besides, U was the support with lower RLE values, most likely because FA tend to remain in the textural pore of the UVM-7 structure in the loading process and was removed during the washing process.

On the other hand, a comparison of RLE values among different impregnation cycles for each support indicated that H and M increased RLE until the third impregnation cycle and then decreased. SBA-15 exhibited the highest RLE value in the second loading cycle. Finally, no significant statistical differences were found for U among different impregnation cycles. According to these results, we considered **H3**, **M3**, **S2** and **U2** as the optimised solids. Those solids were employed in subsequent release and toxicological experiments.

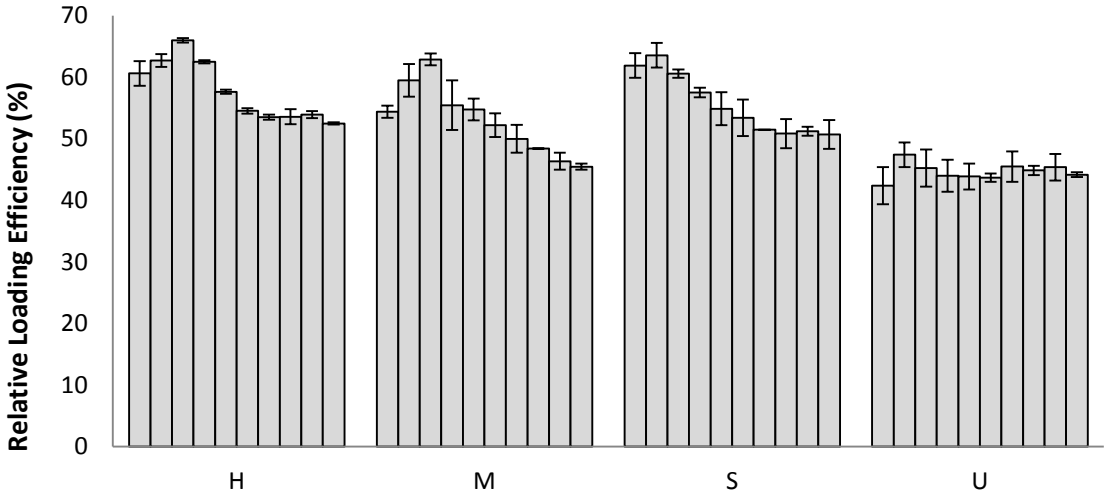

Figure 3. Relative Loading Efficiency for different solids impregnated from 1 to 10 times (ordered sequentially) and functionalized with N3. Hollow Silica Shells (H), MCM-41 (M), SBA-15 (S) and UVM-7 (U). Values are Means±SD, n=3.

478 ***3.3 FA pH-driven controlled release***

479 In order to evaluate the feasibility of different supports to control the bioaccessibility of FA in
480 gastric and intestinal conditions, delivery studies of FA from optimised solids (i.e. H3, M3, S2 and
481 U2) were carried out at pH2 (gastric) and pH 7.5 (intestinal). FA concentrations in the solutions
482 were monitored by HPLC. Figure 4 shows the release behaviour of the four supports loaded with
483 FA and functionalised with N3. For all four supports, a nearly flat baseline was found at pH 2,
484 indicating that FA remained in the voids of the particles without release. It confirmed the
485 capability of the four proposed supports to hinder the release of the vitamin during pass through
486 the stomach. As observed in previous works Bernardos *et al*., 2008; Casasús *et al*., 2008; Pérez-
487 Esteve *et al.*, 2015), there are three mechanisms that favour this zero release: solubility of FA,
488 conformation of polyamines in the gate-like ensemble and the interaction of polyammonium
489 groups with anionic species. At acid pH FA is in its acidic form, exhibiting a very low solubility that
490 hampers FA delivery from the pores (Pérez-Esteve *et al*., 2015). On the other hand, at low pH
491 values (i.e. pH 2) polyamines are transformed to polyammonium groups. This molecular change
492 favours Coulombic repulsions between closely located chains. Tethered polyammonium moieties
493 tend to adopt a rigid-like conformation that pushes them away towards pore openings, blocking
494 the pores and inhibiting completely or partially the release of the vitamin. Moreover,
495 polyammonium groups have the ability to coordinate anions. At pH 2, anions present in the
496 sample (phosphates) interact with the protonated gate-like ensemble creating a superstructure
497 that collaborates to pore blocking. The last two mechanisms are closely interconnected and it is
498 not easy to measure their individual contributions (Bernardos *et al.*, 2008).
499 In contrast, at pH 7.5 (pH of the small intestine), a progressive delivery of FA was observed for all
500 four supports. This different and remarkable behaviour at pH 7.5, when compared to that of pH 2,
501 was due to the effect of pH on both, the solubility of FA and on the conformation of the
502 polyamines. At pH 7.5 FA is in the form of salt, increasing its solubility, and enhancing the delivery

503 from the pore voids to the solution (Zhou & García-Bennett, 2010). Meanwhile polyamines are, at
504 neutral pH, less protonated and their interaction with anions is weaker, favouring pore
505 unblockage. As a consequence, FA was able to be released. This overall behaviour (i.e. no FA
506 delivery at acidic pH and FA delivery at neutral pH) pointed towards the suitability of the designed
507 solids for a selective and controlled delivery of FA in the gastrointestinal tract. At acidic conditions
508 (stomach) the molecular gates would be closed, and therefore no release will be performed. In
509 contrast, after passing to the duodenum the chime could be neutralized as a consequence of the
510 bile and bicarbonate secretion from the pancreatic duct. This neutralization would favour the
511 delivery of the vitamin from the voids, improving the bioaccessibility in the jejunum (pH 7.5),
512 where folic acid is absorbed by a saturable, carrier-mediated, pH and energy-dependent transport
513 mechanism (Wright, Dainty & Finglas, 2007).
514

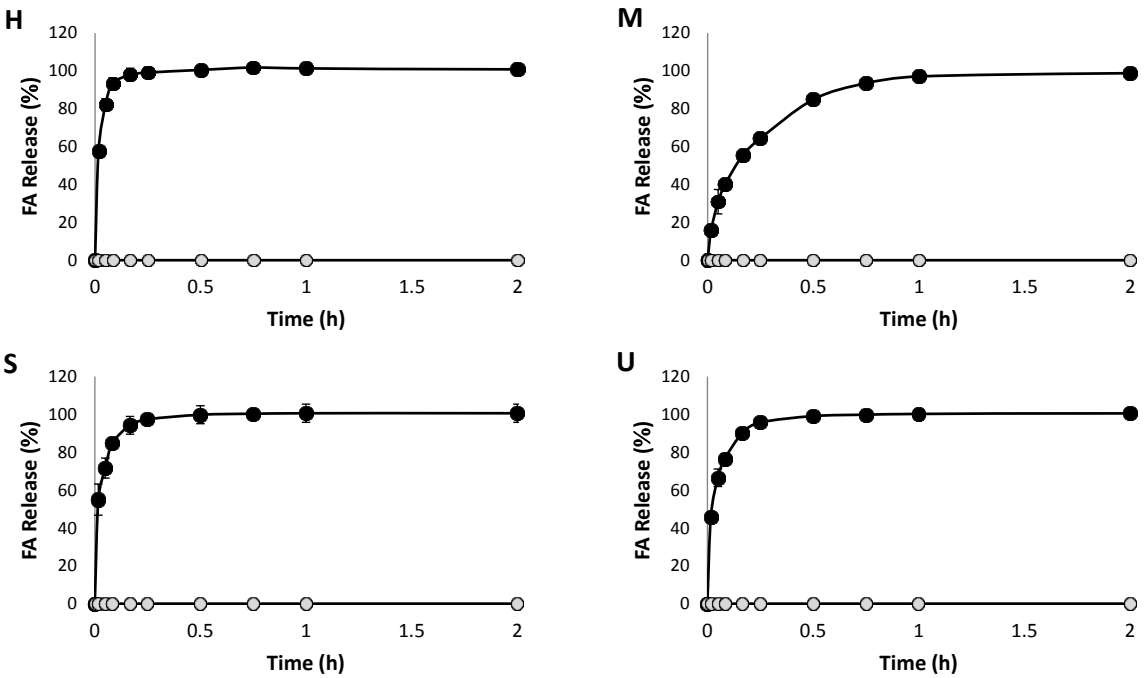

515
516 **Figure 4**. Release profile for different solids in water adjusted at pH 2 (○) and 7.5 (●). Hollow Silica
517 Shells (H), MCM-41 (M), SBA-15 (S) and UVM-7 (U).
518

519 ***3.4 Release kinetics***

520 Besides achieving a remarkable pH-triggered release of FA, we also aimed to evaluate the
521 capability of those systems to control the delivery of the vitamin along time. With this purpose,
522 data from the release kinetics at pH 7.5 were fitted to the Higuchi model. This simple model has
523 been widely, and satisfactorily, applied for describing drug release kinetics from insoluble porous
524 carrier matrixes (Guo, Yang, Cui, Lin & Qu, 2014). It is based on Fickian diffusion processes taking
525 into account the hypotheses that initial drug concentration in the matrix is much higher than drug
526 solubility, that drug diffusion takes place in only one dimension and that drug diffusivity is
527 constant (Dash, Murthy, Nath & Chowdhury, 2010). Figure 5 shows the good fitting of the model
528 to data taken in the first minutes of the delivery, suggesting that in these conditions the delivery
529 of the FA from the pores of different solids is basically a diffusive process. After these times a
530 certain deviation from linearity was found (data not shown).
531 To facilitate interpretation of the data, the release Higuchi rate constant (k_H) of FA from the **H3**,
532 **M3**, **S2** and **U2** supports was calculated. The highest k_H constant was observed for **H3** (k_H=19). S2
533 and **U2** exhibited k_H of 18 and 17 respectively. The lowest k_H value (13) was exhibited by **M3**,
534 being the support that allows a more sustained delivery, and thus the most convenient for
535 modulating FA bioaccessibility along the pass through the small intestine.
536 Higuchi constant has been reported to depend, among other factors, on the diffusivity and
537 solubility of the cargo in the solvent, the tortuosity of the system, the porosity of the matrix and
538 the total amount of compound present in the matrix (Bernardos et al, 2008). In this work the
539 cargo as well as the solvent were the same, and thus, different values were only due to the
540 inorganic support. Having in mind that H is the support with the highest k_H, coinciding with the
541 larger cavity, and that S, U, and M are ordered according to its pore size, the effect of pore size
542 seems to be important to modulate the release kinetics of FA from different supports. The bigger

543 the pore diameter, the easier the entrance of the solution to voids (or main cavity in the case of
544 H), and thus the lower the diffusional problems of FA to escape from the entrapping support.

545

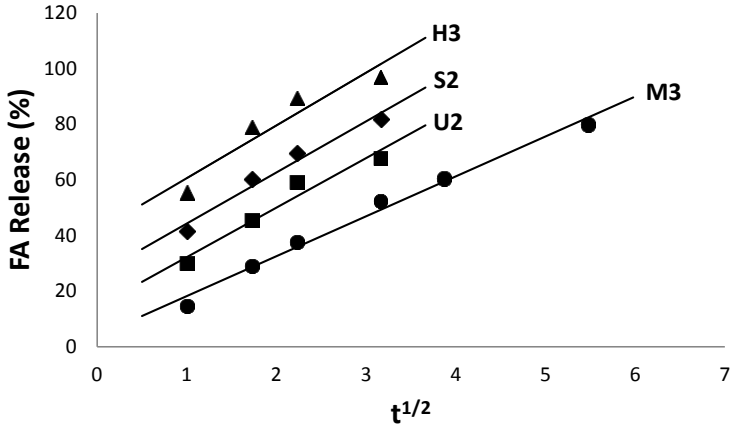

546
547 ***Figure 5***. Higuchi release profile of FA delivered from solids H3, M3, S2 and U2 in aqueous media
548 at pH 7.5
549

550 Figure 5 also allows observing that, with the exception of M3, three of the solids presented a y-
551 interception very superior to 0 value. This phenomenon, called burst release, has been referred to
552 an initial massive release occurring immediately upon placement the delivery system in the
553 release medium. It has been observed in a number of capped mesoporous silica based delivery
554 systems (Bhattacharyya, Wang & Ducheyne, 2012; Radhakrishnan, Gupta, Gnanadhas,
555 Ramamurthy, Chakravortty & Raichur, 2014). Burst release can be favourable in some applications
556 (i.e. encapsulation of aromas, targeted release). However, it is undesired when a sustained
557 release is needed. Having this in mind, M is the support that allows controlling the release of FA
558 during more time and avoids initial burst release.
559 In previous works, some authors have tried to understand the underlying mechanisms of this
560 effect. Potential reasons that may lead to this behaviour are surface characteristics of the host
561 material, sample geometry, host-cargo interaction, morphology and porous structure of dry
562 material among others (Huang & Brazel, 2001). Although the importance of this phenomenon,

563 conclusions are still rare. Thus we have tried to elucidate why different supports with different
564 textural properties exhibited different burst release.
565 Intuitively, it is reasonable to assume that the amount of FA that is delivered during the initial
566 burst release must be dependent on the FA surface directly exposed to the media once the
567 molecular gate was opened at pH=7.5. The practically zero-release at pH=2 and the relatively high
568 density of N-(3-trimethoxysilylpropyl)diethylenetriamine groups (preferentially anchored on the
569 external surface of our solids) allows us to propose that the amount of FA on the external surfaces
570 could be practically discarded. Then, under this last consideration, the FA species must be
571 favourably located inside the pores or cavities present in our silicas. So, in the case of the M
572 support, the initial exposed surface must correspond to the cross-section of the mesopore
573 entrances. Taking into account that the morphology of this M sample is based on the existence of
574 large micrometric particles, a relatively low number of mesopore entrances, and consequently a
575 low initial FA/media interface is expected. In fact, the M support shows the smaller burst release.
576 In a rough way, the U support could be viewed as a nano-version of the MCM-41, with respect to
577 the particle size. This difference strongly affect the average length of the mesopores (although the
578 mesopore sizes are similar, (i.e. their cross-sections). While micrometric mesopore lengths are
579 expected for M supports, pores of nanometric length exist in the U sample. Hence, for a similar
580 mass of support the number of mesopore entrances for the U material must be higher than the
581 entrances present in M support. So, as expected, a higher burst release is detected for U when
582 compared to M support.
583 Although the comparison between M and S supports could be straightforward (similar particle
584 size for both solids, but larger mesopore size for the S), the fact that under the impregnation
585 conditions we have used, the mesopores in the S support remain partially filled with FA (according
586 to N2 adsorption-desorption measurements), make complicated a direct comparison between
587 both solids. In fact, a larger FA surface must be exposed for S support (associated not only to the

588 mesopore entrances but also to the internal mesopore surfaces partially covered by FA). In
589 consequence, as a larger FA/media surface is expected, a more pronounced burst release occurs.
590 Among all supports, is precisely H the one that has a more singular morphology, which is
591 markedly different from the rest of the mesoporous supports. In fact, there is not mesopores in
592 the H support. Once the gate is opened, the invasion of the reaction media inside the internal
593 microcavity must be a very quick process. Due to the fact that the FA should be considered as
594 deposited on the internal cavity but not confined inside pores, a large contact surface is expected,
595 with the subsequent large burst release.
596
597 ***3.5 In vitro biocompatibility tests***
598 In addition to the FA loading and release properties of the different supports, it was also in our
599 aim to assess the biocompatibility of the developed FA carriers. Therefore studies with solids H3,
600 M3, S2 and U2 were performed using HeLa, HTC116, HEPG2 and HK2 cell lines to exclude any
601 toxic effect of the microparticles. Cells were treated with the corresponding capped support for
602 24h at final solid concentrations of 50, 100, 150 and 200 μg/mL. After that time, a cell viability
603 assay using WST-1 was performed. The WST-1 assay is based on the measurement of the
604 absorbance of the stable tetrazolium salt WST-1. This salt is transformed to a soluble formazan
605 derivative by a complex cellular mechanism that occurs primarily at the cell surface. This bio-
606 reduction is largely dependent on the glycolytic production of NAD(P)H in viable cells. Therefore,
607 the amount of formazan dye formed directly correlates to the number of metabolically active cells
608 in the culture. Tetrazolium salts are cleaved to formazan by the succinate-tetrazolium reductase
609 system which belongs to the respiratory chain of the mitochondria, and which is only active in
610 metabolically intact cells.
611 WST-1 cell viability assay indicated that all the cell lines exhibited a high level of cell viability (ca.
612 100% cell proliferation) after 24h upon treatment with solids H3, M3, S2 and U2 up to a

613 concentration of 200 μg/mL (see Supplementary Figure 5). The assay suggested that the
614 developed supports loaded with folic and functionalized with N3 were well tolerated by the cells.
615 Similar levels of biocompatibility of functionalised porous silicas have been reported by other
616 authors (Yuan, Tang, Yang, Zhang, Zhang & Hu, 2011; Mas *et al.*, 2012; Feng, 2013). This high
617 biocompatibility is most likely related with both, the particle size employed and the surface
618 functionalization. He, Zhang, Gao, Shi & Li (2009) studied the cytotoxic effect of spherical
619 mesoporous particles and observed that 190 nm and 420 nm particles showed significant
620 cytotoxicity at concentrations above 25 mg/mL, while micro-scale particles of 1220 nm showed
621 only slight cytotoxicity due to decreased endocytosis. Moreover, the interaction of silanol groups
622 (ca 6% of total surface) with biological molecules, such as cellular membrane lipids and proteins
623 that may strongly interact and eventually modify the structure of these molecules was prevented
624 in our case by the functionalization with organic molecules. In fact, it has been reported that the
625 surface coating of porous silica with organic molecules can increase the biocompatibility and half-
626 lives of cells by more than 10 times compared to bare silica mesoporous supports (Tang, Li &
627 Chen, 2012).
628
629 **4. CONCLUSIONS**
630
631 We have reported herein the use of four different porous silica supports for the design of gated
632 materials able to encapsulate FA, remaining closed at acidic pH (for instance the stomach) yet
633 delivering efficiently the cargo in a neutral pH (for instance in the intestine). Despite the fact that
634 all the designed supports presented a high loading capacity, that all were capable to control the
635 FA release as a function of the pH and that none of them exhibited unspecific toxicity for four
636 different cell lines, one of the supports stands out for showing remarkable advantages in
637 controlling FA bioaccessiblity. Concretely, results reported herein confirm that microparticulated

MCM-41 capped with a simple pH-responsive gate based on polyamines was the only support able to sustain the cargo release for at least one hour. This sustained release is essential to modulate the bioaccessiblity of the vitamin before absorption in the jejunum and thus to avoid problems related to FA absorption peaks that lead into the appearance of untransformed FA in blood. Thus, election of a proper support seems to be essential when planning the design of a smart delivery system.

Acknowledgements

Authors gratefully acknowledge the financial support from the Ministerio de Economía y Competitividad (Projects AGL2012-39597-C02-01, AGL2012-39597-C02-02 and MAT2012-38429-C04-01) and the Generalitat Valenciana (project PROMETEO/2009/016). E.P. and M.R are grateful to the Ministerio de Ciencia e Innovación for their grants (AP2008-00620, AP2010-4369). Electron Microscopy Service of the UPV is also acknowledged.

REFERENCES

Argyo, C., Weiss, V., Bräuchle, C., Bein, T. (2014) Multifunctional mesoporous silica nanoparticles as a universal platform for drug delivery. *Chemistry of Materials,* 26 (1), 435-451.

Aznar, E., Martínez-Máñez, R., Sancenón, F. (2009) Controlled release using mesoporous materials containing gate-like scaffoldings. *Expert Opinion on Drug Delivery,* 6, 643-655.

Baker, H., Thomson, A.D., Feingold, S., Frank, O. (1969) Role of the jejunum in the absorption of folic acid and its polyglutamates. *The American Journal of Clinical Nutrition,* 22(2), 124-132.

Beck, J. S., Vartuli, J. C., Roth, W. J., Leonowicz, M. E., Kresge, C. T., Schmitt, K. D., et al. (1992) A new family of mesoporous molecular sieves prepared with liquid crystal templates. *Journal of the American Chemical Society,* 114 (27), 10834-10843.

Bernardos, A., Aznar, E., Coll, C., Martínez-Mañez, R., Barat, JM., Marcos, M.D., et al. (2008) Controlled release of vitamin B2 using mesoporous materials functionalized with amine-bearing gate-like scaffoldings. *Journal of Controlled Release,* 131, 181-189.

Bhattacharyya, S., Wang, H., Ducheyne, P. (2012) Polymer-coated mesoporous silica nanoparticles for the controlled release of macromolecules. *Acta Biomateralia*, 8, 3429-3435.

Casasús, R., Climent, E., Marcos, M.D., Martínez-Mañez, R., Sancenón, F., Soto, J. et al. (2008) Dual aperture control on pH- and anion-driven supramolecular nanoscopic hybrid gate-like ensembles. *Journal of the American Chemical Society,* 130, 1903-1917.

Comes, M., Aznar, E., Moragues, M., Marcos, M. D., Martínez-Máñez, R., Sancenón, F., et al. (2009) Mesoporous hybrid materials containing nanoscopic "binding pockets" for colorimetric anion signaling in water by using displacement assays. *Chemistry - A European Journal,* 15, 9024-9033.

Dash, S., Murthy, P.N., Nath, L., Chowdhury, P. Kinetic modeling on drug release from controlled drug delivery systems (2010) *Acta Poloniae Pharmaceutica,* 67, 217-223.

Feng, W., Zhou, X., He, C., Qiu, K., Nie, W., Chen, L., et al. (2013) Polyelectrolyte multilayer functionalized mesoporous silica nanoparticles for pH-responsive drug delivery: layer thickness-dependent release profiles and biocompatibility. *Journal of Materials Chemistry B,* 1, 5886-5898.

Grün, M., Unger, K.K., Matsumoto, A., Tsutsumi K. (1999) Novel pathways for the preparation of mesoporous MCM-41 materials: control of porosity and morphology. *Microporous & Mesoporous Materials,* 27, 207-216.

Guo, W., Yang, C., Cui, L., Lin, H., Qu, F. (2014) An enzyme-responsive controlled release system of mesoporous silica coated with konjac oligosaccharide. *Langmuir*, 30, 243-249.

He, C., Yin, L., Tang, C., Yin, C. (2012) Size-dependent absorption mechanism of polymeric nanoparticles for oral delivery of protein drugs. *Biomaterials*, 33, 8569-8578.

He, Q., Zhang, Z., Gao, Y., Shi, J., Li, Y. (2009) Intracellular localization and cytotoxicity of spherical mesoporous silica nano- and microparticles. *Small,* 5, 2722-2729.

Hinterberger, M., Fischer, P. (2013) Folate and Alzheimer: when time matters. *Journal of Neural Transmission,* 120, 211-224.

Huang, X., Brazel, C. S. (2001) On the importance and mechanisms of burst release in matrix-controlled drug delivery systems. *Journal of Controlled Release,* 73, 121-136.

Kotsopoulos J., Kim Y.I., Narod S.A. (2012) Folate and breast cancer: what about high-risk women? *Cancer Causes & Control*, 23, 1405-1420.

Lubecka-Pietruszewska, K., Kaufman-Szymczyk, A., Stefanska, B., Fabianowska-Majewska, K. (2013) Folic acid enforces DNA methylation-mediated transcriptional silencing of PTEN, APC and RARbeta2 tumour suppressor genes in breast cancer. *Biochemical and Biophysical Research Communications,* 430, 623-628.

Mas, N., Agostini, A., Mondragón, L., Bernardos, A., Sancenón, F., Marcos, M.D., et al. (2013) Enzyme-responsive silica mesoporous supports capped with azopyridinium salts for controlled delivery applications. *Chemistry*, 19, 1346-1356.

Mondragón, L., Mas, N., Ferragud, V., de la Torre, C., Agostini, A., Martínez-Máñez, R., et al. (2014) Enzyme-responsive intracellular-controlled release using silica mesoporous nanoparticles capped with ε-poly-L-lysine. *Chemistry*, 20, 5271-5281.

Nasr Hage, C., Jalloul, M., Sabbah, M., Adib, S.M. (2012) Awareness and intake of folic acid for the prevention of neural tube defects among Lebanese women of childbearing age. *Maternal and Child Health Journal***,** 16, 258-265.

Nguyen M.T., Hendrickx M. (2003) Model studies on the stability of folic acid and 5-methyltetrahydrofolic acid degradation during thermal treatment in combination with high

710 hydrostatic pressure. *Journal of Agricultural and Food Chemistry,* 51, 3352-3357.

711 Pérez-Cabero M., Hungría A.B., Morales J.M., Tortajada M., Ramón D., Moragues A., et al.
712 (2012) Interconnected mesopores and high accessibility in UVM-7-like silicas. *Journal of*
713 *Nanoparticle Research*, 14, 1-12.

714 Pérez-Esteve, É., Fuentes A., Coll, C., Acosta, C., Bernardos, A., Amorós, P., et al. (2015)
715 Modulation of folic acid bioaccesibility by encapsulation in pH-responsive gated mesoporous silica
716 particles. *Microporous Mesoporous Materials,* 15, 124-132.

717 Pérez-Esteve, É., Oliver, L., García, L., Nieuwland, M., de Jongh, H., Martínez-Máñez, R., et al.
718 (2014) Incorporation of mesoporous silica particles in gelatine gels: effect of particle type and
719 surface modification on physical properties. *Langmuir*, 30, 6970-6979.

720 Radhakrishnan, K., Gupta, S., Gnanadhas, D.P., Ramamurthy, P.C., Chakravortty, D., Raichur,
721 AM. (2014) Protamine-capped mesoporous silica nanoparticles for biologically triggered drug
722 release. *Particle & Particle Systems Characterization,* 31, 449-458.

723 Tang, F., Li, L., Chen, D. (2012) Mesoporous silica nanoparticles: synthesis, biocompatibility
724 and drug delivery. *Advanced Materials,* 24, 1504-1534.

725 Thielemann, J.P., Girgsdies, F., Schlögl, R., Hesscorresponding, C. (2011) Pore structure and
726 surface area of silica SBA-15: influence of washing and scale-up. *Beilstein Journal of*
727 *Nanotechnology,* 2, 110-118.

728 Wang, S.G., Wu, C.W., Chen, K., Lin, V.S. (2009) Fine-tuning mesochannel orientation of
729 organically functionalized mesoporous silica nanoparticles*. Chemistry - An Asian Journal*, 4, 658-
730 661.

731 Wright, A.J., Dainty, J.R., Finglas, P.M. (2007) Folic acid metabolism in human subjects
732 revisited: potential implications for proposed mandatory folic acid fortification in the UK. *British*
733 *Journal of Nutrition,* 98, 667-675.

734 Yuan, L., Tang, Q., Yang, D., Zhang, J.Z., Zhang, F., Hu, J. (2011) Preparation of pH-responsive
735 mesoporous silica nanoparticles and their application in controlled drug delivery. *The Journal of*
736 *Physical Chemistry C*, 115, 9926-9932.
737 Zhao, D., Huo, Q., Feng, J., Chmelka, B.F., Stucky, G.D. (1998) Nonionic triblock and star
738 diblock copolymer and oligomeric surfactant syntheses of highly ordered, hydrothermally stable,
739 mesoporous silica structures. *Journal of the American Chemical Society*, 120, 6024-6036.
740 Zhou, C., García-Bennett, AE. (2010) Release of folic acid in mesoporous NFM-1 silica. *Journal*
741 *of Nanoscience and Nanotechnology,* 10, 7398-7401.
742 Zhu, Y., Shi, J., Shen, W., Chen, H., Dong, X., Ruan, M. (2005) Preparation of novel hollow
743 mesoporous silica spheres and their sustained-release property. *Nanotechnology*, 16, 2633-2638.
744

745 **Suplementary material - Figures**
746

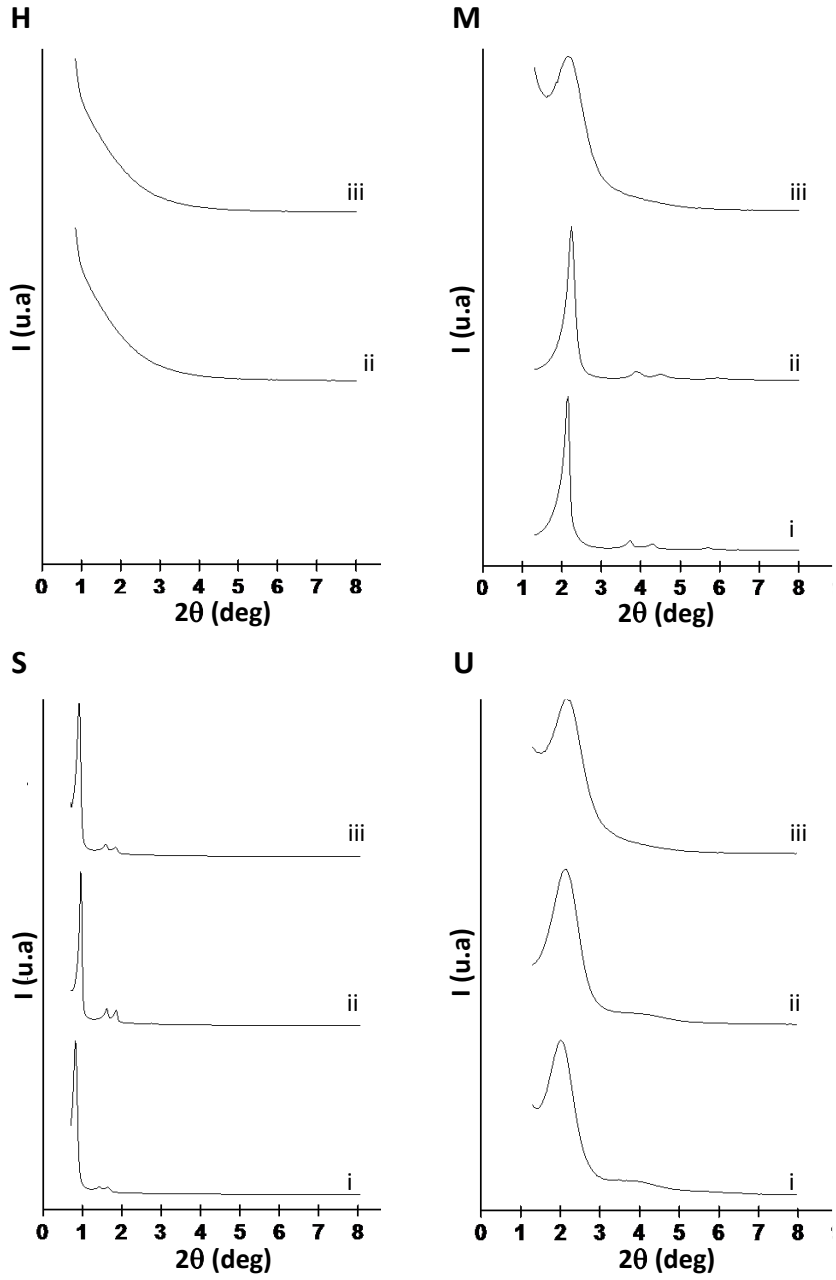

747
748 **Figure S1.** Powder X-ray patterns of the solids i) as synthesized, ii) after calcination and iii) after
749 loading with folic acid and functionalisation with polyamines. Hollow Silica Shells (H), MCM-41
750 (M), SBA-15 (S) and UVM-7 (U).
751

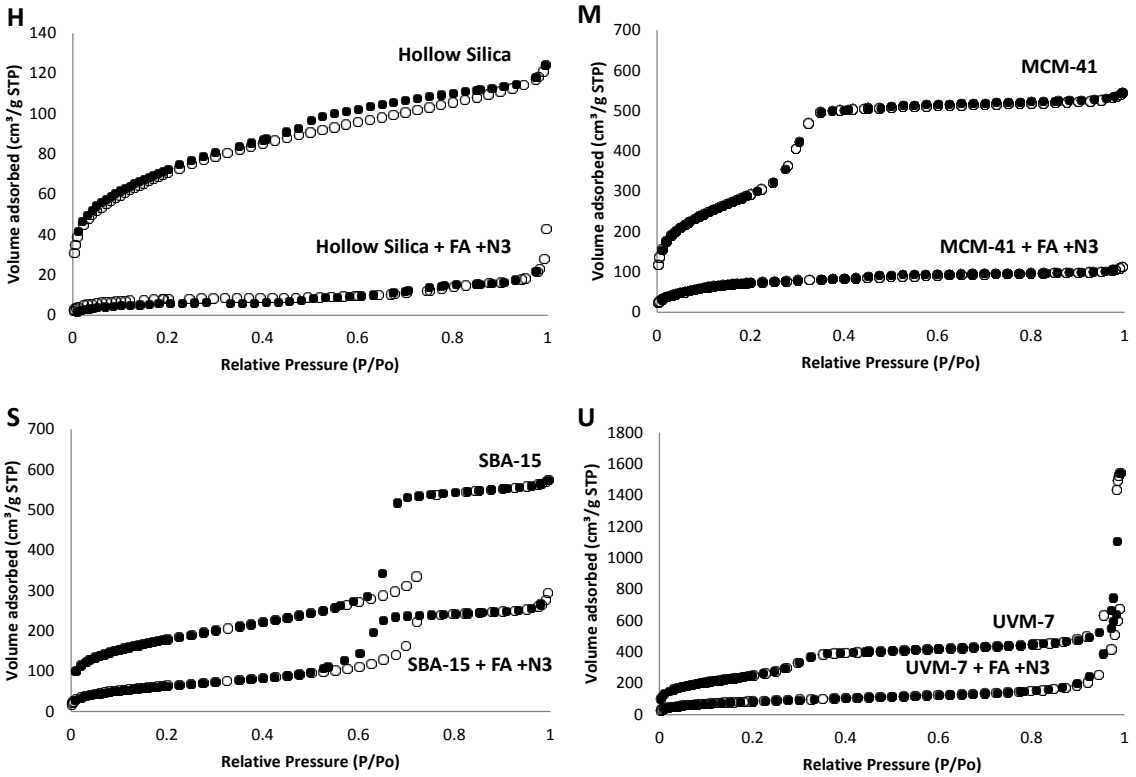

Figure S2. Nitrogen adsorption(○)-desorption(●) isotherms for (H) Hollow Silica Shells, (M) MCM-41, (S) SBA-15 and (U) UVM-7.

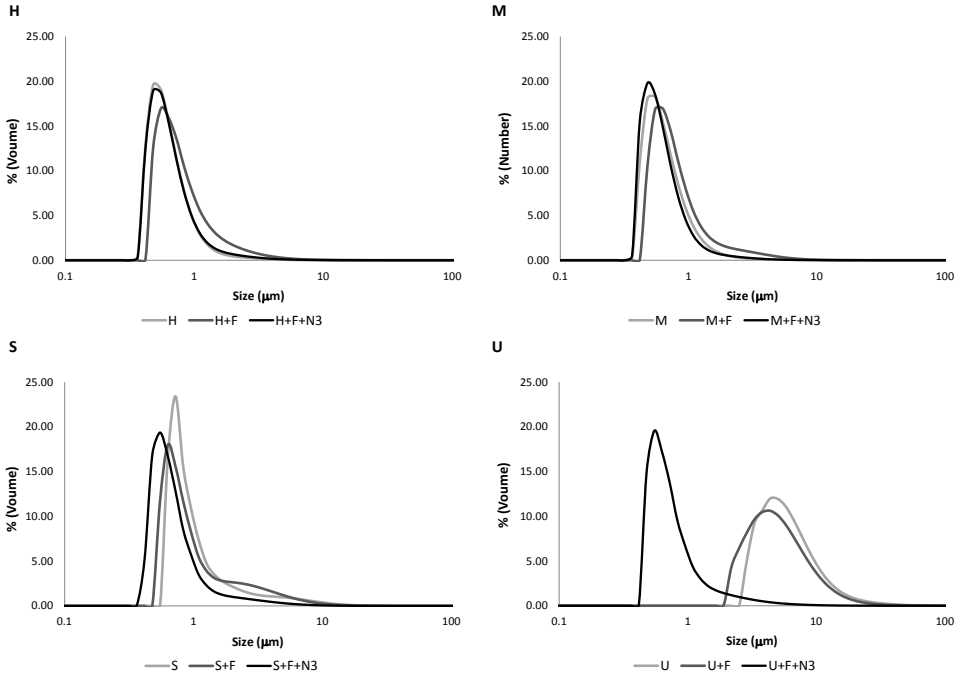

Figure S3. Size distribution of different bare particles (#), particles loaded with FA (#+F) and particles loaded with FA and functionalised with N3 (#+F+N3).

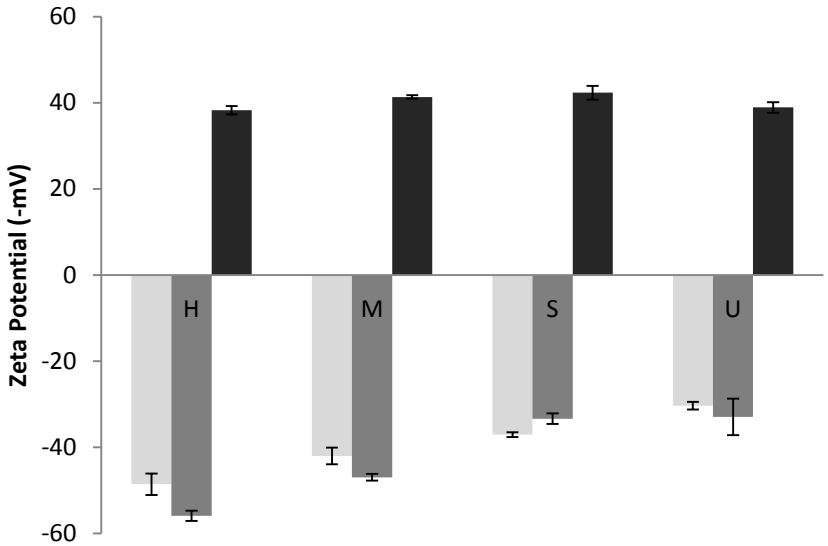

Figure S4. Zeta potential values (Mean±SD) of unloaded supports (light grey), supports loaded with FA (dark grey) and supports loaded with FA and functionalised with N3 (black) dispersed in distilled water. Hollow Silica Shells (H), MCM-41 (M), SBA-15 (S) and UVM-7 (U).

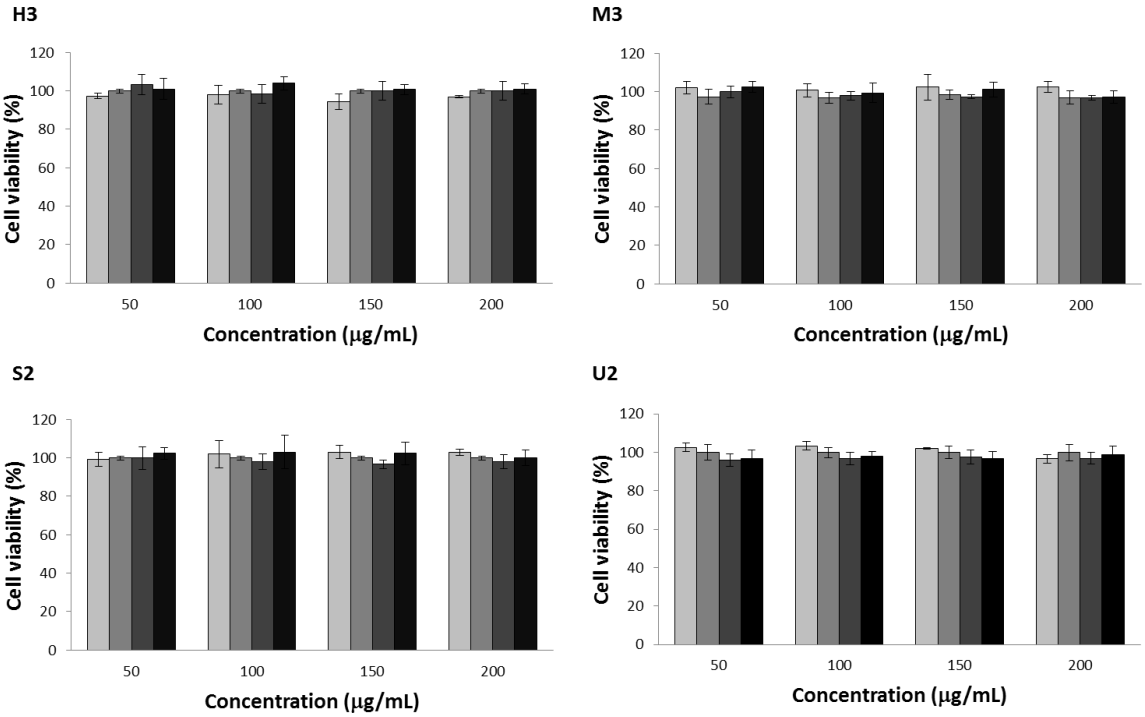

Figure S5. WST-1 cell viability assay. HCT116 (light grey), HEPG2 (medium grey), HK2 (dark grey) and HeLa (black) cells treated with optimized solids at concentrations of 25, 50, 100 and 200 μg/mL for 24 h. Cells were incubated for 24h with optimized solids at the concentrations stated before and cell viability was quantified using the WST-1 reagent.

773 **Suplementary material – Tables**
774
775 **Table S1**. Content (α) of FA and N3 in optimized solids and in solids loaded 10 times. Hollow Silica
776 Shells (H), MCM-41 (M), SBA-15 (S) and UVM-7 (U)

Support	Optimized		Loaded 10 times	
	αFA (mg/g_{solid})	αN3(mg/g_{solid})	αFA(mg/g_{solid})	αN3(mg/g_{solid})
H	125	71	272	59
M	99	75	249	63
S	77	106	264	89
U	95	142	257	118

777
778
779
780
781
782